EDGE ARTICLE

Check for updates

Efficient near-infrared emission benefits from slowing down the internal conversion process†

Mingliang Xie,[a] Yannan Zhou,[a] Huayi Zhou,[a] Chengling Ma,[a] Qikun Sun,[a] Shi-Tong Zhang,[c] Yujian Zhang, [ID] *[b] Wenjun Yang [ID] [a] and Shanfeng Xue [ID] *[a]

Organic deep-red (DR) and near-infrared (NIR) emitters with high photoluminescence quantum yield (PLQY) are rare due to the strong non-radiative (k_{nr}) decay. Here, we report two DR/NIR emitters with high PLQY, **TPANZPyPI** and **TPANZ3PI**. Interestingly, the **TPANZPyPI** film exhibits 46.5% PLQY at 699 nm. Theoretical calculations indicate that **TPANZPyPI** can achieve this high PLQY in the near-infrared emission region due to its small S_1 to S_0 internal conversion (IC) rate. Meanwhile, research has found that, compared to **TPANZ3PI**, **TPANZPyPI** with a more rigid structure can effectively suppress the T_2 to T_1 IC process, which is conducive to higher exciton utilization efficiency (EUE). **TPANZPyPI**'s non-doped OLED shows NIR emission with 4.6% @ 684 nm maximum external quantum efficiency (EQE_{max}). Its doped OLEDs radiate DR with an EQE_{max} of 6.9% @ 666 nm. These EQEs are among the highest values for hybridized local charge transfer state materials emitting more than 640 nm. This work demonstrates for the first time, based on a combination of theory and experiment, that increasing the molecular rigidity can inhibit the excited state IC process in addition to the S_1 to S_0 IC, realizing efficient electroluminescence.

Introduction

Organic light-emitting diodes (OLEDs), a third-generation display technology, have been used in flat panel displays and solid-state lighting devices in recent years. As one of the three primary colors in panchromatic displays, the development of pure organic red emitters lags behind that of blue and green emitters.[1,2] The reason for this is that the energy gap (ΔE) from the first singlet excited state (S_1) to the ground state (S_0) is narrow. According to the law of the energy gap (k_{nr} is directly proportional to $ae^{-b\Delta E}$, where a and b are constants of proportionality),[3,4] it can be seen that the smaller the ΔE, the redder the luminescence and the non-radiative decay rate will exponentially increase with the decrease of ΔE, which means that the non-radiative decay rate (k_{nr}) of red fluorescent materials is much larger than that of blue and green materials. This phenomenon is more significant in the deep-red

(DR) and near-infrared (NIR) domains. To realize efficient luminescence in the DR and even in the NIR, it is necessary to suppress the non-radiative decay process of fluorescent materials.

Non-radiative decay consists of two main aspects: on the one hand, the internal conversion (IC) process from S_1 to S_0, and on the other hand, the intersystem crossing (ISC) process from S_1 to the neighboring triplet state (T). The ISC process is prolonged because the singlet excited and triplet excited states are usually forbidden transitions. Even though singlet excitons can undergo ISC processes, reverse intersystem crossing (RISC) processes may also occur, allowing for the reuse of this portion of singlet excitons. There is no significant heavy atom effect in pure organic fluorescent materials, the IC process is a spin-allowed process between the same states, and the IC rate is usually much larger than the ISC rate. Thus, IC plays a dominant role in non-radiative decay. Therefore, to reduce the IC rate (k_{IC}) is to minimize the non-radiative decay rate. The following equation can describe the IC rate,[5]

$$k_{IC} = 10^{13}e^{-\alpha\Delta E}$$

where α is a rigidity factor influenced by the molecular structure's rigidity, and α will increase with increasing molecular rigidity. Therefore, one way to reduce the IC rate is to increase the rigidity of the molecules. For example, Xu *et al.* reported that the pTPA-DPPZ DR fluorescent material with a large rigid plane achieved a photoluminescence quantum yield (PLQY) of up to

[a]*Key Laboratory of Rubber-Plastics of the Ministry of Education, School of Polymer Science & Engineering, Qingdao University of Science and Technology, Qingdao 266042, P. R. China. E-mail: sfxue@qust.edu.cn*

[b]*Key Laboratory of the Ministry of Education for Advanced Catalysis Materials, Department of Chemistry, Zhejiang Normal University, Yingbin Road No. 688, Jinhua 321004, P. R. China. E-mail: sciencezyj@foxmail.com*

[c]*State Key Laboratory of Supramolecular Structure and Materials, Institute of Theoretical Chemistry, College of Chemistry Jilin University, Changchun 130012, P. R. China*

† Electronic supplementary information (ESI) available: Compound syntheses and characterization, other theoretical calculations, spectra, morphology of films and other device performances. See DOI: https://doi.org/10.1039/d4sc00841c

80.0%.[6] At the same time, the non-doped device prepared with pTPA-DPPZ achieved a maximum external quantum efficiency (EQE) of 12.3% @ 652 nm. However, the PLQY of most non-doped films of DR fluorescent materials with large planes is usually very low, such as the 6.0% and 9.0% PLQY of the non-doped films of ANQDC-MSTA and ANQDC-PSTA reported by Yang *et al.*, and the 14.0% PLQY of the non-doped thin films of TPA-DCPP reported by Wang *et al.*[7,8] There are two main reasons for this. The first is that molecules with large rigidity are usually planar and prone to aggregation-caused quenching (ACQ), leading to lower PLQY. The second is that most of these molecules are thermally activated delayed fluorescence (TADF) materials, whose small overlap between their highest occupied molecular orbitals (HOMOs) and lowest unoccupied molecular orbitals (LUMOs) reduces the oscillator strength and radiative decay rates (k_r) leading to a reduction in the efficiency of the emission.[9–11] The solution to the PLQY reduction due to ACQ is usually to dope these fluorescent materials into suitable host materials at a low concentration, but this usually results in a blue shift emission, making it difficult to achieve DR or NIR emission, and thus achieving efficient DR and NIR emission remains a challenge.

Based on these considerations, this work is premised on the hybridized local charge transfer (HLCT) states with prominent overlapping features between HOMO and LUMO,[12–18] and the rigidity of the molecules is appropriately enhanced in anticipation of achieving high PLQY and high device efficiency. To gain a deeper understanding of the effect of enhanced molecular rigidity on the inhibition of the IC process, in this paper, we have designed and synthesized two novel DR and NIR fluorescent molecules with different rigidity, **TPANZ3PI** and **TPANZPyPI**. The emitters use triphenylamine donors and naphtho[2,3-c][1,2,5]thiadiazole as acceptors. In addition, **TPANZ3PI** uses 1,2,4,5-tetraphenyl-1*H*-imidazole as an auxiliary donor, while **TPANZPyPI** uses 9,10-diphenyl-9*H*-pyreno[4,5-*d*]imidazole as an auxiliary donor (Fig. 1). Among them, the structure of 1,2,4,5-tetraphenyl-1*H*-imidazole has multiple benzene rings that can rotate freely. In comparison, 9,10-diphenyl-9*H*-pyreno[4,5-*d*]

imidazole reduces the number of benzene rings that can rotate freely, making its structure more rigid. Through theoretical calculations, it was found that these emitters have similar electron cloud distributions in the S_1 states (Fig. 1), and their energy level arrangements are identical (Fig. S5†), indicating that they may have similar photophysical properties. The emission peak of the more planar **TPANZPyPI** non-doped film was red-shifted by 33 nm compared to **TPANZ3PI** (666 nm) by testing, located in the NIR region at 699 nm. **TPANZPyPI**'s and **TPANZ3PI**'s PLQYs are 46.5% and 45.5% respectively. To understand this discrepancy more deeply, the IC rate between S_1 and S_0 was calculated and found to be much smaller for **TPANZPyPI** (1.62×10^{11} s^{-1}) than for **TPANZ3PI** (1.73×10^{11} s^{-1}) using the fcclasses and Gaussian software, and the S_1 state of **TPANZPyPI** had more LE state components.[19–22] These results indicate that increasing molecular rigidity is beneficial for inhibiting the IC from S_1 to S_0 while increasing the LE state composition of the molecule and improving PLQY. In addition, the EQEs of the non-doped devices prepared with **TPANZPyPI** and **TPANZ3PI** as the emitting layer are 4.6% @ 684 nm and 4.0% @ 676 nm, making them some of the most efficient devices among DR/NIR non-doped emitters with HLCT characteristics. The exciton utilization efficiency of the **TPANZPyPI** device is 49.5%, higher than that of **TPANZ3PI**'s 43.9%. Based on theoretical calculations, it was found that the IC rate from T_2 to T_1 ($IC_{T_2-T_1}$) of **TPANZPyPI** with a smaller T_2–T_1 energy level difference is lower than that of **TPANZ3PI**'s $IC_{T_2-T_1}$, with rates of 7.54×10^{10} s^{-1} and 3.02×10^{11} s^{-1}, respectively. At the same time, their reverse intersystem crossing (RISC) rates ($RISC_{T_2-S_1}$) are 1.21×10^6 s^{-1} for **TPANZ3PI** and 4.25×10^5 s^{-1} for **TPANZPyPI**. The almost merging of T_2 and T_3 energy levels in **TPANZPyPI** may result in additional RISC channels, with a corresponding RISC rate of 5.53×10^7 s^{-1}. Therefore, enhancing molecular rigidity improves PLQY and suppresses the IC of triplet excitons, achieving higher exciton utilization efficiency. In addition, PPI33PPPBO was used as the host to achieve the EQE of 6.9% @ 666 nm in the **TPANZPyPI** doped device, which is one of the highest values of HLCT DR emission.
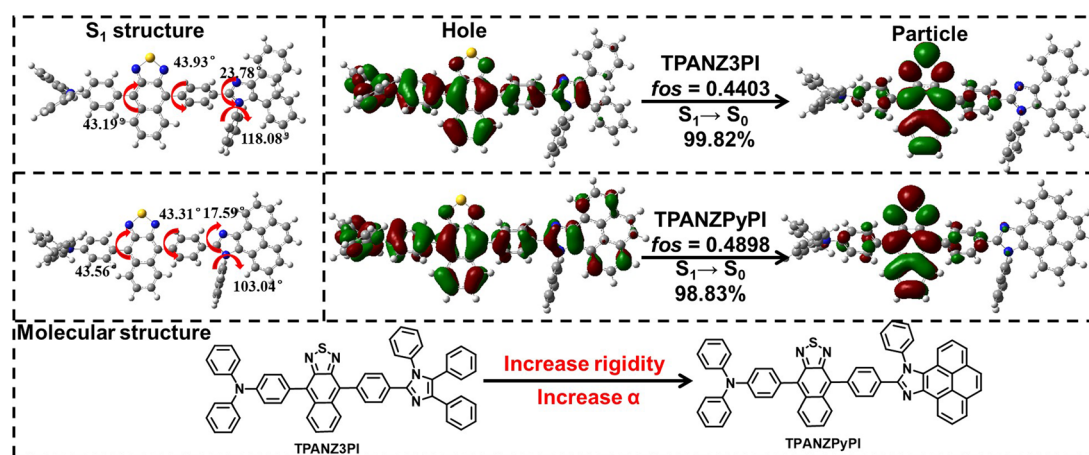

Fig. 1 Molecular structures, optimized singlet excited state (S_1) structure, and electron cloud distributions of **TPANZ3PI** and **TPANZPyPI**. *fos* is the oscillator strength.

Results and discussion

Synthesis and characterization

The target molecules **TPANZPyPI** and **TPANZ3PI** were efficiently synthesized (see Scheme 1 and S1 in the ESI† for detailed synthesis). Due to the molecule's rigidity and poor solubility, the ^{13}C NMR spectrum of **TPANZPyPI** could not be obtained. Still, suitable ^{1}H NMR spectra and high-resolution mass spectrometry (HRMS) were available, proving the product's characterization and purity (Fig. S1–S3†). **TPANZPyPI** and **TPANZ3PI** are obtained at a sublimation temperature of over 250 °C under a 1.0×10^{-5} Pa pressure, exhibiting high thermal stability. Their decomposition temperatures (T_d, equivalent to 5% weight loss, Fig. S4†) are 496 °C for **TPANZPyPI** and 328 °C for **TPANZ3PI**, which is beneficial for the preparation of OLED devices. Besides, the glass transition temperatures (T_g) of **TPANZPyPI** and **TPANZ3PI** are 184 °C and 158 °C, respectively. The electrochemical behavior of emitters was also tested using cyclic voltammetry (Fig. S4†). The reduction potentials of **TPANZPyPI** and **TPANZ3PI** are −1.20 V, and the oxidation potentials are 0.46 V and 0.60 V, respectively. The corresponding LUMO energy levels are estimated to be approximately −3.52 eV, while the HOMO energy levels are −5.05 eV and −5.19 eV, respectively.

Theoretical calculations

Fig. 1 shows the molecular geometry and electron cloud distribution of the optimized S_1 states of the emitters. The torsion angle of **TPANZPyPI** is generally smaller than that of **TPANZ3PI** at the same position, indicating that **TPANZPyPI** has a planarized structure, which is beneficial for increasing the oscillator strength of molecules. Meanwhile, these emitters' hole and particle distributions are similar, with the holes mainly concentrated on the triphenylamine and naphthothiadiazole portions and only a small portion extending to the imidazole portion. On the other hand, the particle is focused primarily on the naphthothiadiazole acceptor, with only a small portion extending into the adjacent benzene ring. This hole and particle exhibit overlapping and separated HLCT features in the S_1 state. In addition, we also calculated the proportion of LE and CT states in the S_1 state of these two molecules. The CT/LE components of **TPANZPyPI** and **TPANZ3PI** are 65.435%/35.565% and 66.806%/33.194%, respectively. Among them, the S_1 states of **TPANZPyPI** have more LE components that help to achieve higher luminescence efficiency. Their emission energies are similar at 2.08 eV and 2.06 eV, respectively (Table S1†). These similar results imply that their luminescence properties may be similar. Furthermore, the corresponding excited state energy level arrangements (Tables S1 and S2, and Fig. S5†) were calculated with the ground state structures of these emitters. It can be found that the energy level difference between T_1 and S_1 ($\Delta E_{T_1-S_1}$) of these emitters exceeds 1.0 eV, which implies that the RISC process from T_1 to S_1 cannot occur and that the $\Delta E_{T_2-T_1}$ for **TPANZPyPI** and **TPANZ3PI** is 1.129 eV and 1.206 eV, respectively. Most importantly, these emitters' $2T_1 < S_1$, suggesting the triplet–triplet annihilation mechanism is ruled out.

In order to understand the effect of enhanced molecular rigidity on the structural changes between the ground and excited states, the root mean square deviation (RMSD) values and corresponding reorganization energies (λ) between the ground (S_0) and excited states (S_1) were calculated, as shown in Fig. 2.[6] In Fig. 2, it can be observed that **TPANZPyPI** has a smaller RMSD value and reorganization energy, indicating that increasing molecular rigidity can suppress structural changes, which may reduce energy loss during the excitation process caused by excited state changes. To explain this difference, the Huang–Rhys factor (HRF) was calculated using fcclasses to quantify the coupling strength between structural changes and vibration modes. For **TPANZ3PI** and **TPANZPyPI**, the HRF of $S_1 \rightarrow S_0$ is mainly composed of low-frequency rotational and torsional vibration modes (below 50 cm^{-1}), with large HRF values as high as 4.94 and 1.73, respectively. **TPANZPyPI** has smaller HRF values due to the near absence of low-frequency rotational and torsional vibrational modes in 9,10-diphenyl-9H-pyreno[4,5-d]imidazole compared to 1,2,4,5-tetraphenyl-1H-imidazole in **TPANZ3PI** (Fig. S6†). These results indicate that **TPANZPyPI** has a more rigid structure, and according to our previous discussion, a more rigid structure would be favorable for inhibiting the IC process. To this end, we first qualitatively calculated the internal conversion rates ($k_{IC(S_1-S_0)}$) between these emitters S_1 and S_0 at room temperature. We found that the $k_{IC(S_1-S_0)}$ of **TPANZPyPI** is 1.62×10^{11} s^{-1}, while
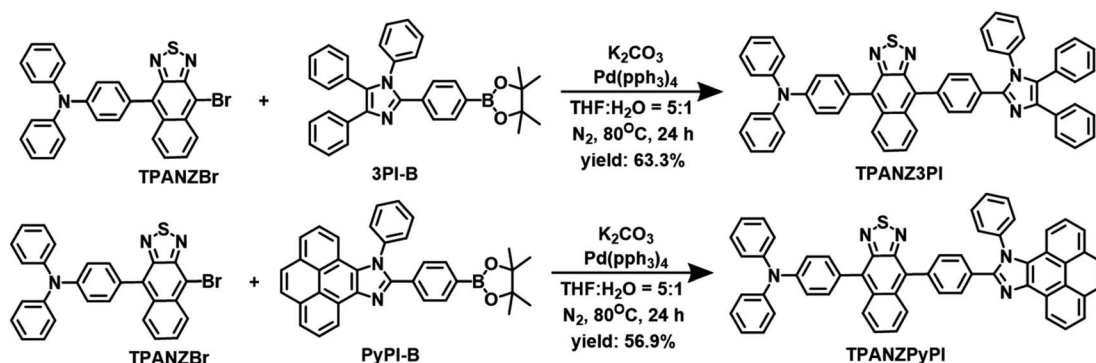
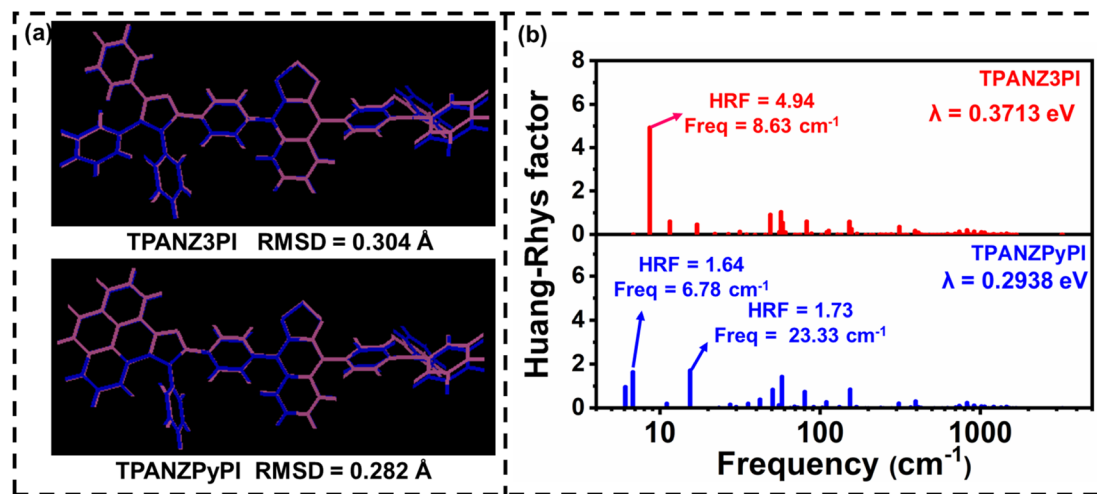**Scheme 1** The synthesis routes of TPANZPyPI and TPANZ3PI.

Fig. 2 (a) The RMSD value between S_1 and S_0, where the S_1 structure is mauve and S_0 is blue, and (b) the Huang–Rhys factors *versus* frequencies.

the $k_{IC(S_1-S_0)}$ of **TPANZ3PI** is 1.73×10^{11} s^{-1}, which is consistent with our expectations. We also believe that enhancing molecular rigidity can help suppress the IC process of triplet-excited states. For this purpose, the IC rate between T_1 and T_2 of these emitters was also qualitatively calculated at room temperature. Although the energy level difference between T_1 and T_2 is more minor for **TPANZPyPI** (Fig. S5†), the $k_{IC(T_2-T_1)}$ rate is smaller than for **TPANZ3PI**, where $k_{IC(T_2-T_1,\ \textbf{TPANZPyPI})} = 7.54 \times 10^{10}$ s^{-1}, while $k_{IC(T_2-T_1,\ \textbf{TPANZ3PI})} = 3.02 \times 10^{11}$ s^{-1}. The lower IC rate is more favorable for keeping electrically generated triplet excitons at the T_2 energy level. Although the energy level differences in T_1 and T_2 are so large, there are IC rates up to 10^{10} to 10^{11} s^{-1} orders of magnitude. And the usual RISC rates for high-energy triplet to singlet states of pure organic molecules are 10^7 to 10^8 s^{-1} orders of magnitude.[23] Therefore, pure organic molecules usually consider only the RISC process from T_2 to S_1. Thus, the RISC rate from T_2 to S_1 was calculated, and the RISC rate for **TPANZ3PI** was 1.21×10^6 s^{-1}, and the RISC rate for **TPANZPyPI** was 4.25×10^5 s^{-1}. However, considering that the small T_3–T_2 gap of **TPANZPyPI** supports IC and the dynamic equilibrium of reverse IC through vibration coupling, it is reasonable for triplet excitons to be converted into singlet excitons through thermal exciton channels ($T_2/T_3 \rightarrow S_1$). Therefore, the RISC rate corresponding to **TPANZPyPI** is 5.53×10^7 s^{-1} between T_3 and S_1. Combining a smaller IC rate of triplets with a larger RISC rate compared to **TPANZ3PI**, **TPANZPyPI** is expected to have higher exciton utilization efficiency.

Photophysical properties

Fig. 3a shows the ultraviolet-visible (UV-vis) absorption and photoluminescence (PL) spectra of **TPANZPyPI** and **TPANZ3PI** in dilute solutions of THF (10^{-5} M) and pure films. Detailed data are shown in Table 1. The emitters show similar absorption in the pure films and THF, but the absorption peak in the films is red-shifted compared to that in THF, which may be attributed to the aggregation of molecules in the film state. The absorption

bands at about 300–400 nm are mainly due to molecular π–π^* transition, whereas the absorption bands after 400 nm originate from the emitter backbone's intramolecular charge transfer (ICT). The emission in THF/film is 698/671 nm and 699/666 nm for **TPANZPyPI** and **TPANZ3PI**, respectively. The solvatochromic test is shown in Fig. S7,† and detailed data are recorded in Table S3.† **TPANZPyPI** and **TPANZ3PI** showed a redshift of 91 nm and 90 nm from low-polarity hexane to high-polarity acetone, respectively, which indicates they have similar excited state properties. The redshifts in the different solutions indicate that the CT component enhances with increasing polarity, consistent with a gradual decrease in PLQY (Table S3†). However, it is worth noting that **TPANZ3PI** and **TPANZPyPI** have PLQYs of 46.5% @ 699 nm and 45.5% @ 666 nm in the pure film, respectively. Especially **TPANZPyPI** has a very high PLQY, which is rare in the NIR field. This result is consistent with theoretical calculations. In addition, the Lippert–Mataga solvation model was applied to the emitters. In Fig. 3c, the relationship between the Stokes shift of two emitters and solvent polarity shows two fitting lines. The dipole moments at low polarity ($f < 0.15$) are 11.85 D and 11.28 D, respectively, which are larger than typical pure LE excited states (~8 D). The dipole moment in the higher polarity environment ($f > 0.15$) is 18.36 D and 19.24 D, respectively. The transient PL spectra exhibit a single exponential lifetime curve in solvents of different polarities (Fig. S8†) or pure film states (Fig. 3d), indicating only one hybrid state in S_1. Considering the electron cloud distribution of S_1, these emitters should be considered HLCT emitters.

Electroluminescent devices

Given the excellent photophysical properties of emitters, their electroluminescence properties were further investigated. Non-doped devices were first prepared with the structure of ITO/ HATCN (20 nm)/TAPC (35 nm)/TCTA (10 nm)/EML (20 nm)/ TPBi (60 nm)/LiF (1 nm)/Al (100 nm), in which HATCN (1,4,5,8,9,11-hexaazatriphenylenehexacarbonitrile) is the hole-injection layer, TAPC (1,1-bis[[di-4-tolylamino)phenyl]
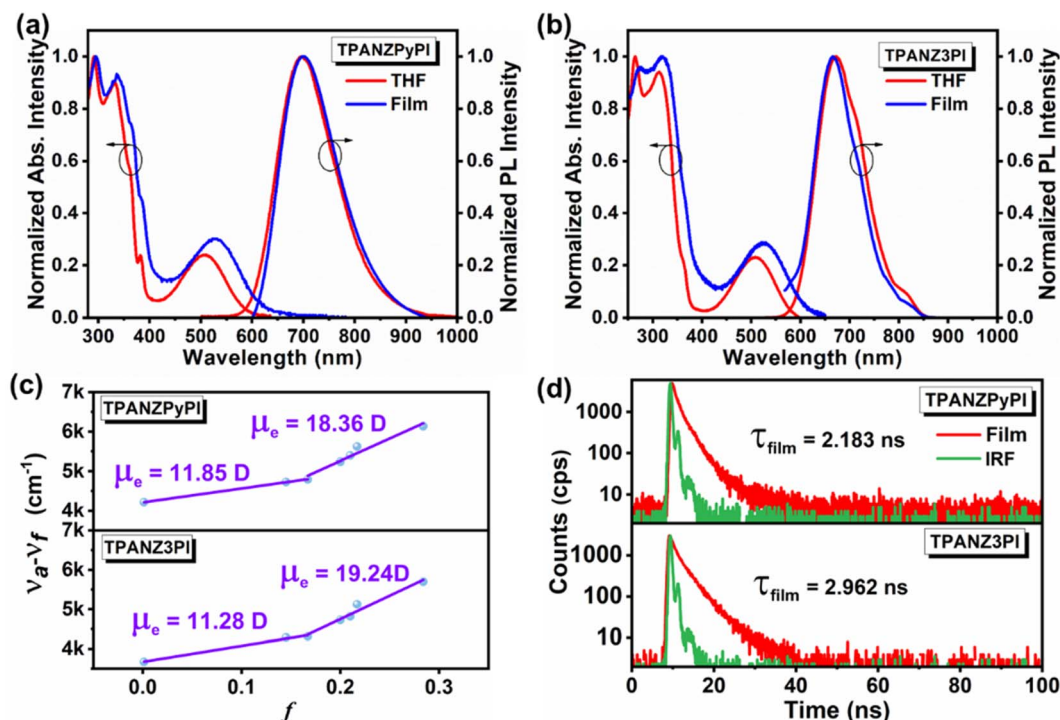
Fig. 3 The UV–vis absorption spectra and the PL spectra of the films and solutions (10^{-5} M) of (a) **TPANZPyPI** and (b) **TPANZ3PI**; (c) linear fitting of the Lippert–Mataga model, and (d) the transient PL decay spectra of **TPANZPyPI** and **TPANZ3PI** in films.

Table 1 The photophysical data of **TPANZ3PI** and **TPANZPyPI** films

Compound	$\lambda_{abs}{}^{a}$ [nm]	$\lambda_{em}{}^{b}$ [nm]	$\Phi_F{}^{c}$ [%]	τ^{d} [ns]	$k_r{}^{e}$ [10^7 s^{-1}]	$k_{nr}{}^{e}$ [10^7 s^{-1}]	$\Phi_F{}^{f}$ [%]
TPANZPyPI	295/336/527	699	46.5	2.18	21.30	24.51	66.1
TPANZ3PI	273/316/525	666	45.5	2.96	15.36	18.40	74.5

[a] Absorption peaks of the neat film. [b] Maximum emission wavelength of the neat film. [c] Absolute PLQY of the neat film. [d] Fluorescence lifetime of the neat film. [e] k_r and k_{nr} for the neat film ($k_r = \Phi_F/\tau$, $k_{nr} = (1 - \Phi_F)/\tau$). [f] 10 wt% emitters in PPI33PPPBO host absolute PLQY.

cyclohexane) is the hole-transport layer, TCTA (tris(4-carbazoyl-9-ylphenyl)amine) is the hole-transport layer and electron-blocking layer, and TPBi (2,2′,2″-(1,3,5-benzinetriyl)-tris(1-phenyl-1-H-benzimidazole)) is the electron-transport layer and hole-blocking layer (Fig. S9†). The corresponding data is recorded in Table 2. The non-doped **TPANZPyPI** OLED shows NIR emission at 684 nm with a color coordinate of (0.69, 0.30) and provides a maximum EQE of 4.6%, which is comparable to the DR to NIR emission of state-of-the-art non-doped OLEDs

with HLCT characteristics. However, the device with **TPANZ3PI** as the emission layer has an emission peak of 676nm and a maximum EQE of 4.0%. Due to the similar molecular structures of **TPANZ3PI** and **TPANZPyPI**, to qualitatively compare the exciton utilization efficiency of their non-doped devices, the optical output coupling efficiency is assumed to be 0.2, and thus the exciton utilization efficiency of **TPANZPyPI** and **TPANZ3PI** is 49.5% and 43.9%, respectively. This result matches the theoretical calculations and proves that the appropriate

Table 2 EL performances of the OLEDs based on **TPANZPyPI** and **TPANZ3PI**

EML	$V_{turn-on}{}^{a}$ [V]	$LE_{max}{}^{b}$ [cd A^{-1}]	$PE_{max}{}^{c}$ [lm W^{-1}]	$EQE_{max}{}^{d}$ [%]	$L_{max}{}^{e}$ [cd m^{-2}]	$\lambda_{EL,max}{}^{f}$ [nm]	CIE $[x,y]^{g}$
TPANZPyPI	3.0	0.93	0.60	4.6	4756	684	(0.693, 0.302)
TPANZ3PI	3.0	0.96	0.93	4.0	4495	676	(0.692, 0.305)
PPI33PPPBO: **TPANZPyPI**	3.0	3.30	3.46	6.9	8072	666	(0.675, 0.323)
PPI33PPPBO: **TPANZ3PI**	2.9	3.03	3.28	6.1	6467	666	(0.678, 0.323)

[a] $V_{turn-on}$: turn-on voltage at 1 cd m^{-2}. [b] LE_{max}: maximum current efficiency. [c] PE_{max}: maximum power efficiency. [d] EQE_{max}: maximum external quantum efficiency. [e] L_{max}: maximum luminance. [f] $\lambda_{EL,max}$: electroluminescence peak. [g] CIE: Commission Internationale de l'Eclairage coordinates.
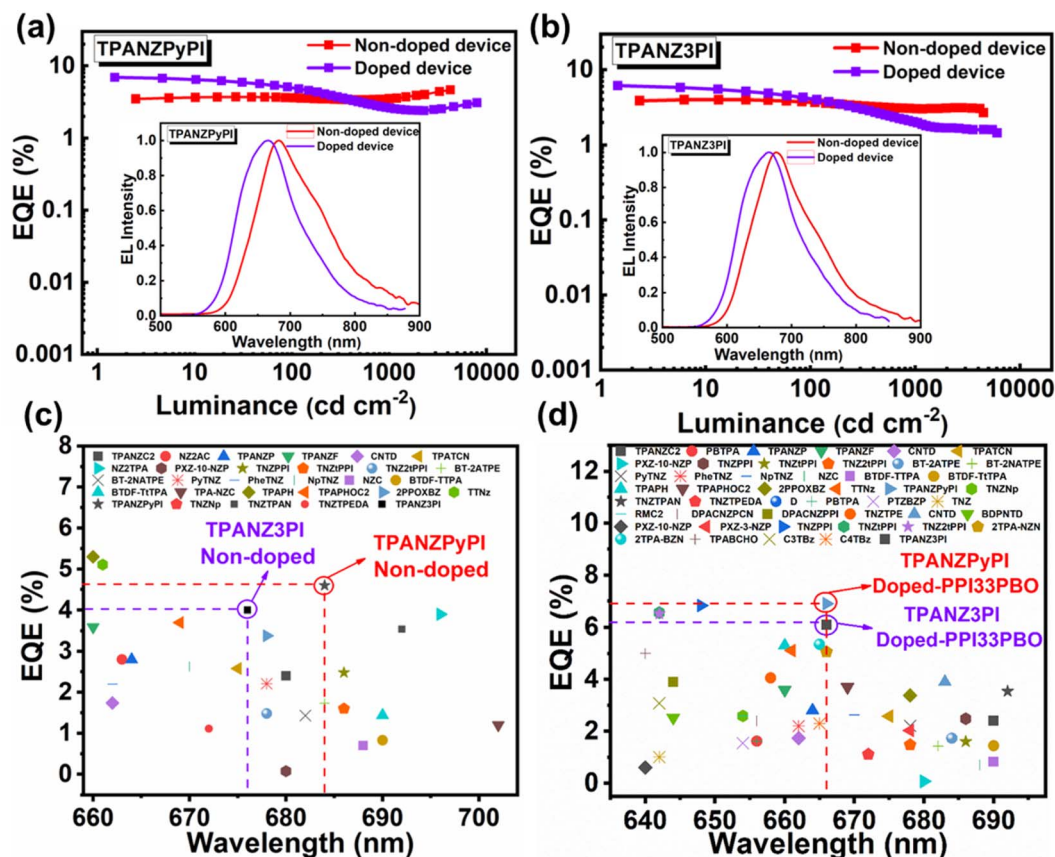
Fig. 4 (a) and (b) Luminance−EQE plots with EL spectra inserted, (c) reported maximum EQE of red non-doped HLCT OLEDs with electroluminescence peaks ranging from 660 to 710 nm, (d) reported maximum EQE of red doped HLCT OLEDs with electroluminescence peak ranging from 640 to 700 nm.

enhancement of molecular rigidity is beneficial to reduce the internal conversion process of the excited state and realize higher exciton utilization efficiency. However, it is worth noting that the EQE curves of the devices of **TPANZPyPI** show an upward trend at high voltages. This may be attributed to the fact that at high voltages, the internal conversion from T_2 to T_1 is limited, and the density of the T_2 and T_3 excitons is elevated, further facilitating the RISC process and improving the efficiency of the devices. There's another possibility that the suppression of T_1 exciton density growth at high current density, as stated in the literature, reduces the likelihood of singlet–triplet annihilate (STA) occurrence, thereby enabling the device to achieve higher EQE at high current densities.[24] Because the energy level arrangement of these emitters ($2T_1 < S_1$, Fig. S5†) and the current density-luminance curve of the device have a linear relationship (Fig. S11†), which excludes TTA behavior, the increase of EQE at high current density is also independent of TTA. The curves of the spectra at different voltages and the corresponding color coordinates did not change significantly (Fig. S12 and Table S4†), ruling out that the device efficiency improvement is due to the change of the composite region.

Further investigations were conducted on the electroluminescence performance of emitter doped organic light-emitting devices (ITO/HATCN (20 nm)/TAPC (40 nm)/TCTA (20 nm)/host:**TPANZPyPI** (10 wt%, 20 nm)/TPBI (50 nm)/LiF (1 nm)/Al (100 nm), where the host is our previously reported PPI33PPPBO).[25] The device structure is shown in Fig. S9,† and the emission spectra of the PPI33PPPBO film and absorption spectra of the **TPANZPyPI** and **TPANZ3PI** films are shown in Fig. S10.† Compared with non-doped organic electroluminescent devices, these doped devices emit a blue shift but significantly improve the electroluminescence efficiency, consistent with the doped films' high PLQY (Table 1). Doped in PPI33PPPBO, the **TPANZPyPI** and **TPANZ3PI** devices all show DR emission with peaks at 666 nm and excellent EL performance, with the maximum luminance of 8072 cd m^{-2} and 6467 cd m^{-2}, and the maximum EQE of 6.90% and 6.1%, respectively, which is one of the highest values reported so far for DR HLCT OLEDs (Fig. 4).

Conclusions

In summary, we synthesized and characterized two DR and NIR molecules, **TPANZ3PI** and **TPANZPyPI**, with different rigid structures. Theoretical calculations reveal that increasing the molecular rigidity can inhibit the IC process from S_1 to S_0, which improves the photoluminescence efficiency and shows

Edge Article

NIR emission in neat films. Moreover, increasing the molecular rigidity also slows the internal conversion process between excited states, thus enabling this HLCT material to achieve higher exciton utilization efficiency and superior electroluminescence performance. **TPANZPyPI** non-doped devices with greater rigidity have achieved higher EQE and exciton utilization efficiency than **TPANZ3PI** with values of 4.6%/49.5% @ 684 nm and 4.0%/43.9% @ 676 nm, respectively. The doping devices of these two emitters achieved 666 nm DR emission, with an EQE of 6.9% for **TPANZPyPI** and 6.1% for **TPANZ3PI**, respectively. To our knowledge, these results are among the highest EL efficiencies reported for HLCT NIR/DR emission. These results suggest the moderate increase in molecular rigidity is a practical approach to designing high-performance DR/NIR fluorescent materials.

Data availability

All data supporting this study are available from article and ESI.†

Author contributions

Mingliang Xie conducted the synthesis and the photophysical characterizations of the materials. Yannan Zhou and Chengling Ma fabricated the OLED for the materials and estimated the OLED performances. Huayi Zhou is responsible for the basic testing and analysis of thermal and electrochemical properties. Shi-Tong Zhang and Qikun Sun did the theoretical calculations. Mingliang Xie wrote the paper, and all the authors revised it. Shanfeng Xue, Yujian Zhang and Wenjun Yang supervised the whole work.

Conflicts of interest

There are no conflicts to declare.

Acknowledgements

Notes and references

1 Y. Xu, P. Xu, D. Hu and Y. Ma, *Chem. Soc. Rev.*, 2021, **50**, 1030–1069.

2 Y. Liu, C. Li, Z. Ren, S. Yan and M. R. Bryce, *Nat. Rev. Mater.*, 2018, **3**, 18020.

3 S. Sharma and A. K. Pal, *J. Mater. Chem. C*, 2022, **10**, 15681–15707.

4 F. Liu, Y. Tan, H. Liu, X. Tang, L. Gao, C. Du, J. Min, H. Jina and P. Lu, *J. Mater. Chem. C*, 2020, **8**, 6883–6890.

5 J.-X. Chen, K. Wang, C.-J. Zheng, M. Zhang, Y.-Z. Shi, S.-L. Tao, H. Lin, W. Liu, W.-W. Tao, X.-M. Ou and X.-H. Zhang, *Adv. Sci.*, 2018, 1800436.

6 B. Zhao, H. Wang, C. Han, P. Ma, Z. Li, P. Chang and H. Xu, *Angew. Chem., Int. Ed.*, 2020, **132**, 19204–19209.

7 X. Gong, C.-H. Lu, W.-K. Lee, P. Li, Y.-H. Huang, Z. Chen, L. Zhan, C.-C. Wu, S. Gong and C. Yang, *Chem. Eng. J.*, 2021, **405**, 126663.

8 S. Wang, X. Yan, Z. Cheng, H. Zhang, Y. Liu and Y. Wang, *Angew. Chem., Int. Ed.*, 2015, **54**, 13068–13072.

9 J.-X. Chen, Y.-F. Xiao, K. Wang, D. Sun, X.-C. Fan, X. Zhang, M. Zhang, Y.-Z. Shi, J. Yu, F.-X. Geng, C.-S. Lee and X.-H. Zhang, *Angew. Chem., Int. Ed.*, 2021, **60**, 2478–2484.

10 T. Yang, Z. Cheng, Z. Li, J. Liang, Y. Xu, C. Li and Y. Wang, *Adv. Funct. Mater.*, 2020, 2002681.

11 Z. Cai, X. Wu, H. Liu, J. Guo, D. Yang, D. Ma, Z. Zhao and B. Z. Tang, *Angew. Chem., Int. Ed.*, 2021, **60**, 23635–23640.

12 H. Zhang, G. Li, X. Guo, K. Zhang, B. Zhang, X. Guo, Y. Li, J. Fan, Z. Wang, D. Ma and B. Z. Tang, *Angew. Chem., Int. Ed.*, 2021, **60**, 1–8.

13 S. Xiao, Y. Gao, R. Wang, H. Liu, W. Li, C. Zhou, S. Xue, S.-T. Zhang, B. Yang and Y. Ma, *Chem. Eng. J.*, 2022, **440**, 135911.

14 M. Xie, T. Li, C. Liu, C. Ma, S. Zhang, G. Liu, Q. Sun, S.-T. Zhang, W. Yang and S. Xue, *Chem. Eng. J.*, 2023, **472**, 144950.

15 T. Liu, X. Chen, J. Zhao, W. Wei, Z. Mao, W. Wu, S. Jiao, Y. Liu, Z. Yang and Z. Chi, *Chem. Sci.*, 2021, **12**, 5171–5176.

16 J. Zhu, G. Liu, X. Lian, J.-H. Pang, M.-D. Li, Y. Wang and Q.-X. Tong, *J. Mater. Chem. C*, 2022, **10**, 8684–8693.

17 Z. Zhong, X. Zhu, X. Wang, Y. Zheng, S. Geng, Z. Zhou, X. J. Feng, Z. Zhao and H. Lu, *Adv. Funct. Mater.*, 2022, **32**, 2112969.

18 Q. Wan, J. Tong, B. Zhang, Y. Li, Z. Wang and B. Z. Tang, *Adv. Opt. Mater.*, 2019, 1901520.

19 J. Cerezo and F. Santoro, *J. Comput. Chem.*, 2023, **44**, 626–643.

20 F. Neese, *Wiley Interdiscip. Rev. Comput. Mol. Sci.*, 2018, **8**, e1327.

21 F. Neese, F. Wennmohs, U. Becker and C. Riplinger, *J. Chem. Phys.*, 2020, **152**, 224108.

22 A. Humeniuk, M. Bužančić, J. Hoche, J. Cerezo, R. Mitrić, F. Santoro and V. Bonačić-Koutecký, *J. Chem. Phys.*, 2020, **152**, 054107.

23 J. Li, M. Zhang, T. Li, D. Guo, T. Tian and H. Zhang, *J. Mater. Chem. C*, 2022, **10**, 13124–13136.

24 Y. Zhang, M. Whited, M. E. Thompson and S. R. Forrest, Singlet–triplet quenching in high intensity fluorescent organic light emitting diodes, *Chem. Phys. Lett.*, 2010, **495**, 161–165.

25 C. Liu, T. Li, M. Sun, M. Xie, Y. Zhou, W. Feng, Q. Sun, S.-T. Zhang, S. Xue and W. Yang, *Adv. Funct. Mater.*, 2023, **33**, 2215066.